Synthesis of trans-pinocarveol from oxidation of β-pinene using multifunctional heterogeneous catalysts

Sánchez-Velandia, Julián E.; Valdivieso, Laura M.; Martínez O, Fernando; Mejía, Sol M.; Villa, Aída L.; Wärnå, Johan; Murzin, Dmitry Yu

Published in:
Molecular Catalysis

DOI:
10.1016/j.mcat.2023.113104

Published: 15/04/2023

Document Version
Final published version

Document License
CC BY

Molecular Catalysis 541 (2023) 113104

Contents lists available at ScienceDirect

Molecular Catalysis

journal homepage: www.journals.elsevier.com/molecular-catalysis

Synthesis of *trans*-pinocarveol from oxidation of β-pinene using multifunctional heterogeneous catalysts

Julián E. Sánchez-Velandia [a,b,*], Laura M. Valdivieso [c], Fernando Martínez O [c], Sol M. Mejía [b], Aída L. Villa [d], Johan Wärnå [e], Dmitry Yu. Murzin [e]

[a] Departamento de Química Inorgánica y Orgánica, Grupo de Investigación en Química Supramolecular y Sostenible, Universidad Jaume I, Castellón de la Plana, Spain
[b] Departamento de Química, Facultad de Ciencias, Grupo de Investigación Fitoquímica Universidad Javeriana, Pontificia Universidad Javeriana, Bogotá, Colombia
[c] Centro de Investigaciones en Catálisis, Escuela de Química, Universidad Industrial de Santander, Bucaramanga, Colombia
[d] Environmental Catalysis Research Group, Chemical Engineering Department, Universidad de Antioquia, Medellín, Colombia
[e] Faculty of Science and Engineering, Åbo Akademi University, Turku, Finland

ARTICLE INFO

Keywords:
Allylic oxidation
Multifunctional catalysts
Monoterpenes
Biomass

ABSTRACT

In this contribution, several multifunctional heterogeneous catalysts comprising an acid and a metal function were synthesized by wetness impregnation and tested in the allylic oxidation (with hydrogen peroxide as an oxidizing agent) of β-pinene, a monoterpene which is present in several plants being one of the main constituents of the turpentine oil. Among the tested catalysts, the material containing Pd with a heteropolyacid supported on SBA-15 (Pd/HPA-300/SBA-15) was the best catalyst achieving the most promising results (up to 65% of yield to *trans*-pinocarveol). Independent on the Pd loading (0.5 wt% or 1.0 wt%) and calcination temperature of the heteropolyacid supported on SBA-15 (200°C-300°C), selectivity to *trans*-pinocarveol remained the same. At the same time the calcination temperature affected conversion, Pd dispersion, acidity, and the surface area. When the support changed to amorphous SiO_2 (with a lower surface area $< 200\ m^2/g$) both selectivity and conversion decreased dramatically to values lower than 20%. Weak Brønsted acid sited together with a typical particles shape favors formation and selectivity to the desired product. Laboratory scaling up of β-pinene oxidation was performed (up to 10 mL) achieving the same results in terms of activity and selectivity thereby showing a possibility of a practical implementation of the proposed catalytic system. Kinetic modelling of the reaction was performed to elucidate the determining steps involving in the allylic oxidation of β-pinene. The catalysts showed to be robust since it can be used up to 3 times without apparent changes in both selectivity and conversion but with a slight presence of lixiviation.

1. Introduction

Valorization of biomass is currently gaining an increasing attention being able to mitigate an otherwise negative impact on the environment associated with conventional manufacturing of fuels and chemicals [1–3]. Biomass can be a feedstock for a variety of products at the same time allowing an adequate disposal of biodegradable waste. Monoterpenes, natural renewable materials, could be specially interesting for the synthesis of high-added value chemicals [4–6]. In particular, *α*- and *β*-pinene are bicyclic hydrocarbons having a double bond which makes them initial platforms for the synthesis of potential substances with applications in fine chemistry, polymers and pharmaceuticals [7,8]. Oxidation of pinenes gives a wide range of substances including allylic oxidation products as well as epoxides.

Oxygenated terpenes are applied for the synthesis of fine chemicals or as chiral building blocks for fragrances, flavor as well as pharmaceutical products (as citral, menthol, sandalwood fragrance or Taxol) [6,9]. Driving selectivity to a specific product of selective oxidation is a still a great challenge therefore novel selective catalysts are required. In oxidation of β-pinene different products can be obtained (Fig. 1). Among them, mainly *trans*-pinocarveol (Pcvol), pinocamphone (Pcam), myrtenol (Mol) and myrtenal were synthesized [10,11]. These compounds can be used for different important applications in both fine and pharmaceutical chemistry. For example, myrtenol is a potential biomarker to be

* Corresponding author at: Departamento de Química Inorgánica y Orgánica, Grupo de Investigación en Química Supramolecular y Sostenible, Universidad Jaume I, Castellón de la Plana, Spain.
E-mail address: velandia@uji.es (J.E. Sánchez-Velandia).

https://doi.org/10.1016/j.mcat.2023.113104
Received 21 December 2022; Received in revised form 18 March 2023; Accepted 20 March 2023
Available online 29 March 2023

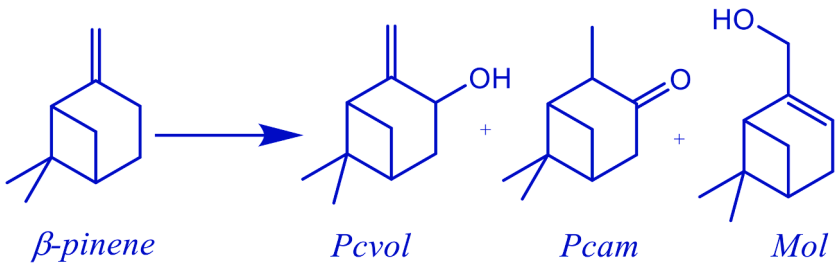

Fig. 1. Allylic oxidation of β-pinene onto *trans*-pinocarveol, pinocamphone and myrtenol.

used as an anxiolytic precursor because of its anti-inflammatory effects [12,13]. Myrtenal also exhibits anti-nociceptive and anti-inflammatory properties [14]. On the other hand, *trans*-pinocarveol was reported to be the main product after β-pinene is subjected to the fungus strain *Aspergillus niger NC1M 612* and to *Armillariella mellea* (honey fungus) [15]. Because of its reactivity and the chemical structure, *trans*-pinocarveol could be transformed into a variety of products with potential applications in fine chemistry.

Chemoselectivity of allylic oxidation reaction can be achieved and controlled with an adequate palladium catalyst as well as by choosing the correct experimental conditions [10]. Interestingly, a Pd homogeneous catalyst was reported for the synthesis of allylic oxidation products from β-pinene at relative mild reaction conditions. $PdCl_2$ was tested with H_2O_2 as an oxidizing agent and acetonitrile as a solvent reaching conversion of *ca.* 58% with selectivity to a variety of oxidized products of almost 60% [16]. On the other hand, oxidation of several alkenes including β-pinene was performed using a copper-aluminum mixed oxide together with L-proline and the results showed that *trans*-pinocarveol can be obtained with a yield of 81% using tert-butyl hydroperoxide (TBHP) as an oxidizing agent (1.0 mmol of β-pinene, 6.0 mmol of TBHP, 82°C, 24 h and acetonitrile as a solvent, 60 mg of catalyst); however, no information about the catalyst recycling was reported [17]. On the other hand, Nb supported on MCM-41 was also tested in the oxidation of β-pinene with hydrogen peroxide as an oxidizing agent (3.75 mol of pinene, 15.9 mmol of H_2O_2, 60°C, 8 h, acetonitrile as solvent) giving 96% of conversion with a selectivity to the oxidation products of 44% [11]. Application of hydrogen peroxide slightly decreased the conversion (93%) but considerably increased selectivity to the oxidation products (62%). However, selectivity to the desired pinocarveol was lower (up to 32%) in comparison with the previous reports. π-Allypaladium complexes were also used to obtain *trans*-pinocarveol from β-pinene with *tert*-butylhydroperoxide, $MnO_2(acac)_2$ and $CHCl_3$ as a solvent [18]. From these reports, it can be concluded that Pd could have a major effect in the selective allylic oxidation of terpenes. Although monoterpenes oxidation catalyzed by Pd based catalysts has been already studied, the control of selectivity is still one of the main challenges. Thus, the design and testing of a new family of catalysts should be proposed.

Among heterogeneous Pd catalysts, Pd/TiO_2 showed to be effective for the allylic oxidation of cyclohexane to produce cyclohexanone and cyclohexanol (KA oil) which is important for the production of nylon [19]. Synergistic catalysts exhibiting both acid and metal functions have been reported as an excellent combination for the oxidation of olefins because of a high redox potential of metal species [20,21]. In this way, noble-metal promotion with heteropolyacids was observed as an effective catalyst for the Wacker type catalytic oxidation of cyclohexene to cyclohexanone [22].

Regarding different metals that have been tested for the allylic oxidation of this monoterpene, Pd was reported to be one of the most interesting metal to be applied as a catalyst for this reaction. However, there are only few studies on utilization of this metal in heterogeneous supported catalysts. Considering that previously high values of conversion and selectivity were obtained with homogeneous catalysts, in this contribution, we used Pd on a heterogeneous matrix of heteropolyacid, which was itself deposited on a mesoporous material. Several parameters such as the amount of catalyst, pinene-to-hydrogen peroxide ratio and stability were evaluated in allylic oxidation of β-pinene. In addition, kinetic modelling was included to further elucidate the main reaction pathways.

2. Experimental

2.1. Materials

The following materials were used as received: co-polymer P-123 (Aldrich,40%wt), HCl (Scharlau, 37 wt%), tetraethylortosilicate (Aldrich, TEOS, 98% wt), Keggin's like heteropolyacid (Acros Organics, $H_3O_{40}PW_{12}.xH_2O$), $Pd(CH_3COO)_2$ (Aldrich, 47 wt% of Pd), β-pinene (Aldrich, 98 wt%), H_2O_2 (Aldrich, 50 % wt), acetone (Aldrich).

2.2. Synthesis of catalysts

2.2.1. Pd/HPA/SBA-15

In a typical procedure, SBA-15 was synthesized using a well-known protocol reported in the literature [23]. Namely, 2.1765 g of triblock co-poymer (P123, Aldrich, PEG 40% w/w) was dispersed in 16 g of deionized water and 62 g of HCl (2 M). Then, 5 g of TEOS was added dropwise and stirred (450 rpm) at 40°C for 24 h. The hydrothermal synthesis was performed in an autoclave at 105°C for 48 h. Finally, the solid was washed with deionized water and calcined at 550°C for 24 h giving a white solid. Incorporation of the heteropolyacid and Pd was performed using sequential impregnation. For this purpose, 0.1 g of the heteropolyacid ($H_3O_{40}PW_{12}.xH_2O$, named as HPA) was added to 0.6 g of SBA-15 (previously calcined at 550°C for 1 h) together with 30 mL of deionized water. The mixture was constantly stirred and left for 1 h. Then, the solid was dried at 100°C for 17 h and calcined at 200°C for 3 h in static air. This material was coded as HPA/SBA-15.

Impregnation of HPA/SBA-15 with $Pd(CH_3COO)_2$ was performed using 1 wt% of palladium acetate as a Pd precursor (with respect to HPA/SBA-15) dissolved in 30 mL of tetrahydrofuran. The mixture was stirred for 1 h and then dried at 100°C for 18 h. Finally, the solid was calcined at 200°C for 3 h in static air. It has been reported that temperatures between 200 and 300°C are enough to decompose palladium acetate [24].

Two additional palladium containing catalysts were synthesized for the purposes of comparison. One contained a lower amount of palladium (Pd(0.5)/HPA/SBA-15) while the other one was obtained after calcination of HPA/SBA-15 at 300° (Pd/HPA-300/SBA-15).

Pd/SBA-15 was also prepared using the following procedure: 1 wt. % of the same Pd precursor as above was added to 0.2 g of SBA-15 and the mixture was constantly stirred using 30 mL of ethyl acetate as a solvent. Then, the material was dried for 18 h at 100°C and calcined for 3 h at 200°C. Reproducibility and repeatability of the synthesis of these materials was also verified by comparison of different batches in the catalytic reaction or at least by analyzing textural properties by nitrogen physisorption, as well as acidity by FTIR spectroscopy.

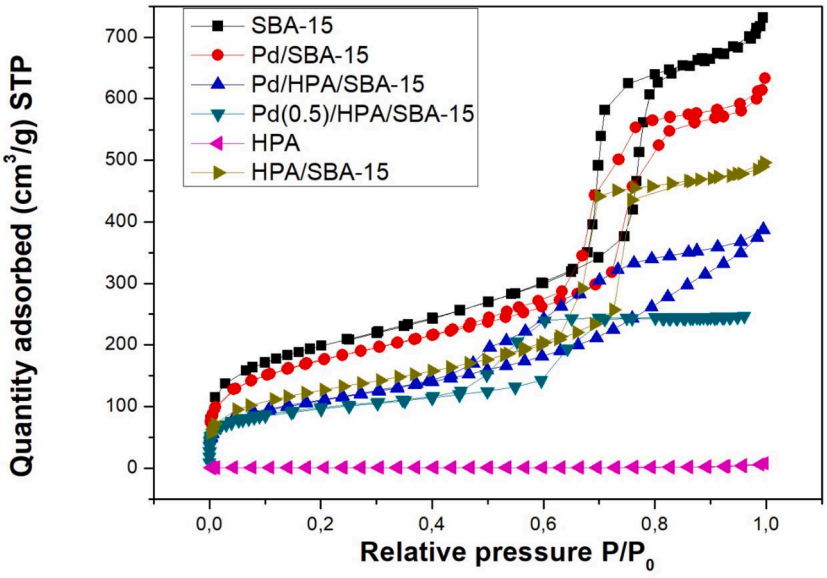

Fig. 2. Adsorption-desorption isotherms of some selected heterogeneous catalysts.

Table 1
Surface properties of some selected heterogeneous catalysts.

Catalyst	Surface area (m^2/g)	Pore volume (cm^3/g)	Dp (nm)	Surface coverage θ*	Pd (%)**
SBA-15	721	1.1	6	-	0.0
HPA	3	-	-	-	0.0
Pd/SBA-15	615	0.9	7	-	1.0
HPA/SBA-15	436	0.8	8	0.1040	0.0
Pd/HPA-300/SBA-15	390	0.6	7	0.1160	1.6
Pd/HPA/SBA-15	569	0.9	6	0.0794	1.8
Pd(0.5)/HPA/SBA-15	335	0.4	5	0.1350	0.5

* θ is the nominal HPA surface coverage which can be calculated as follows: $\theta = Area_{HPA}\ (N_A\ wHPA)(MW_{HPA})^{-1}(S_{BET})^{-1}$ where $Area_{HPA}$ stands for the cross-sectional area of hexagonal close packed array of Keggin units, N_A is the Avogadro's number, wHPA is the mass fraction of HPA and S_{BET} is the surface area. [7] In all cases the HPA loading was 15 wt%

** Estimated Pd amount by using emission spectroscopy.

2.2.2. *Pd/HPA/SiO$_2$*

Synthesis of this material was carried out in the same way as explained in Section 2.2.1 (also including the calcination temperature). A change of the support in this synthesis by using amorphous silica (A_{BET}: 200 m^2/g) rather than SBA-15 was done with the aim to explore the effect of the support in the synthesis of alcohols by allylic oxidation of monoterpenes.

2.3. *Characterization of materials*

Nitrogen adsorption/desorption isotherms were measured on a Micromeritics Tristar 3000 apparatus at -196°C. Before analysis, the samples were degassed under vacuum at 150°C for 12 h. The specific surface area was determined from the linear part (0 - 0.23 P/P_0) of the BET plot. The total pore volume was measured from the isotherms at $P/P_0 = 0.95$ and the mean pore diameter was determined by the BJH method applied to the desorption branch. XPS spectra were acquired using XPS/ISS/UPS-Acenteno platform from SPECS with the energy analyzer PHOIBOS 150 2D-DLD. The measurements were performed with a monochromatic X-ray Al Ka (FOCUS 500) operated at 100 W. The pass energy of hemispheric analyzer was fixed at 100 eV for the general spectra and 20 eV for the high-resolution spectra. The compensation of the surface charge was controlled using Flood-Gun (FG 15/40-PS FG 500) which was operated at 94 μA-3.6 eV. Analysis of XPS spectra was performed by using CASA XPS software [25]. Pyridine analysis was performed in a Jasco FTIR equipment. Typically, 50 mg of a sample were degasified at 120°C during 12 h. Then, adsorption of pyridine was performed at 150°C at 15°C/min; afterwards, pulses of pyridine were carried out with the aim to obtain the same pressure in each part of the equipment. Desorption was performed at 25°C, 50°C, 150°C, 250°C and 350°C. The strength of the acid sites was defined as follows: weak (150°C), medium (250°C) and strong (350°C). Brønsted to Lewis ratio (B/L) was calculated from the absolute values of the peak areas at 1450 and 1550 cm^{-1} which correspond to Lewis and Brønsted bands, respectively [8]. Scanning Electronic Microscopy was used to determine morphology of some selected materials. For this purpose, the samples were fixed in a graphite film and mixed in a gold thin recovery (Denton Vacuum Desk IV). Then, the samples were analyzed in a JEOL JSM 6490 LV equipment. Complementary elemental analysis was performed by means of SEM-EDX using an X-ray microprobe (reference INCA Penta-FETx3 Oxford instruments). Pd content was determined by using emission spectroscopy in an Agilent 240FS AA equipment.

2.4. *Catalytic activity*

Catalytic reactions were performed in 10 mL batch reactors under magnetic stirring. In a typical experiment, the selected amount of the catalyst was added to different concentrations of β-pinene and hydrogen peroxide (H_2O_2, 50% wt) in acetone. Prior to reactions the catalysts were activated at 100°C to remove humidity and grinded to a particle size of <45 μm ensuring no diffusional problems related to internal mass transfer. Efficient stirring at 450 rpm and a low particle size ensured absence of external mass transfer limitations. The products were quantified by GC Agilent 6890 with an FID and HP-1 column (100 m ×250

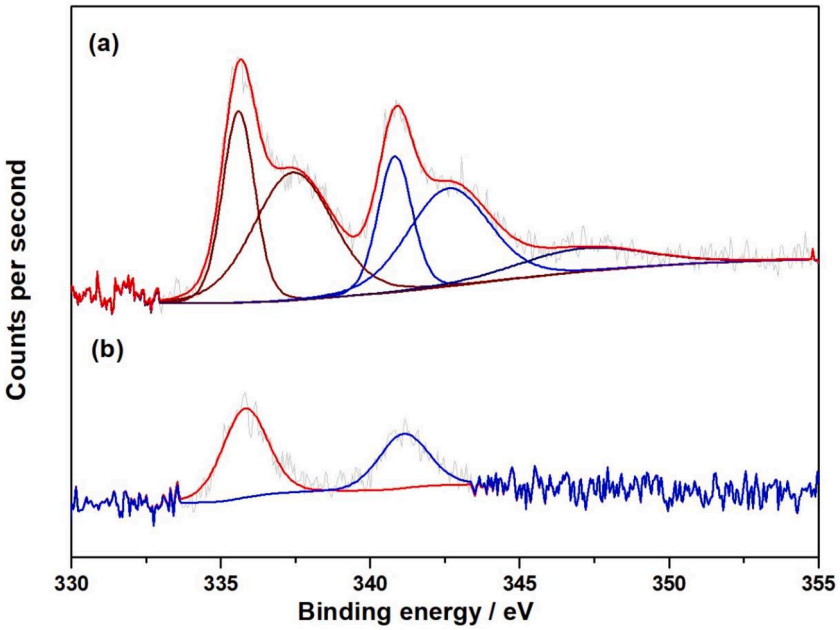

Fig. 3. High- resolution Pd XPS spectra for (a) Pd/SBA-15 and (b) Pd(0.5%)/HPA/SBA-15.

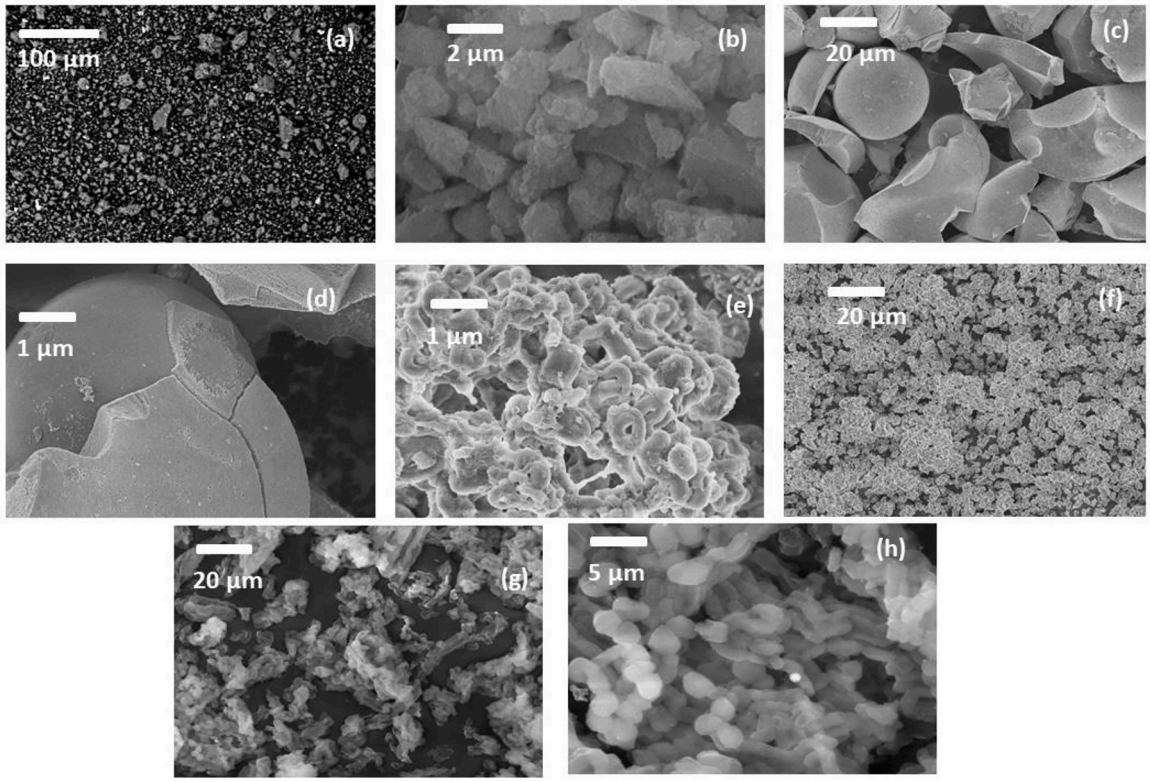

Fig. 4. SEM images of some selected materials: (a) Pd/HPA/SBA-15, (b) Pd(0.5)/HPA/SBA-15, (c) and (d)Pd/HPA/SiO_2, (e) and (f) Pd/SBA-15, (g) and (h) Pd/HPA-300/SBA-15.

µm x 0.5 µm). The carrier gas was N_2 (24 mL min^{-1}) and the split ratio was 15:1. The oven temperature was kept at 50 °C for 3 min being thereafter raised to 180 °C at 15 °C/min ramping and maintained for 2 min. Toluene was used as an internal standard. Typical chromatograms before and after reaction are presented in Supplementary Information (Figs. S1 and S2). The mass balance was verified comparing the areas of the chromatograms after and before the catalytic reactions giving the mass balance closure of 95–100%. The products were identified by comparison with authentic samples and using mass spectrometry. The mass spectra are shown in Supplementary Information (Figs. S3–S5).

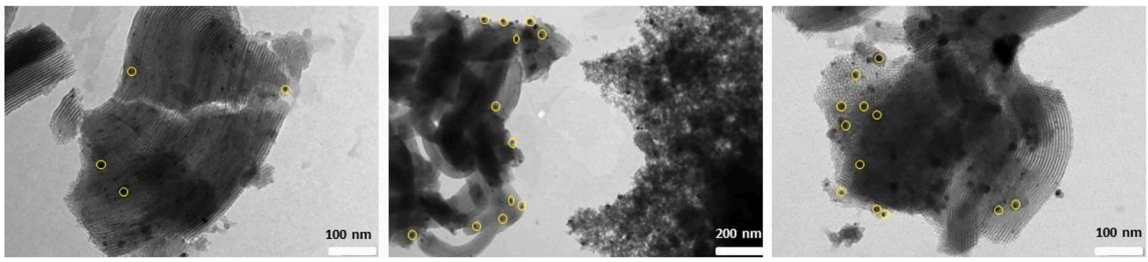

Fig. 5. TEM images for Pd/HPA/SBA-15 catalyst. Some Pd particles are highlighted in yellow.

3. Results and discussion

3.1. Catalyst characterization

3.1.1. Textural properties

Fig. 2 and Table 1 show the adsorption-desorption isotherms and the surface area/pore volume/pore size for the Pd based catalysts, respectively. In the case of SBA-15, an isotherm type IV with a H2 hysteresis typical of mesoporous catalysts is visible. A large surface area (721 m^2/g) was obtained for the parent material. The isotherm suggesting cylindrical pores is characteristic for SBA-15. As should be expected, the heteropolyacid *per se* exhibits a very low area (only 3 m^2/g). The surface area of Pd/SBA-15 is lower than for SBA-15 (721 vs 615 m^2/g), which suggests changes in porosity during impregnation. In the same way, geometry and the size of the pores were different (Fig. 2), namely hysteresis seems to be wider in the case of SBA-15 in comparison with Pd/SBA-15. It has been suggested by molecular simulation studies that as the length of cylindrical pore increases the width of the hysteresis loop also increases [26], which is the same trend observed in this work for SBA-15 and Pd/SBA-15.

Interestingly, when Pd was incorporated on HPA/SBA-15, the surface area decreased considerably to 390 m^2/g, which could be attributed to the blockage of the pores and to a slight increase of the crystallite size. When the calcination temperature of the Pd precursor decreased to 200°C (Pd/HPA/SBA-15 catalyst), a decrease of the surface area was also obtained. For HPA/SBA-15, which surface area decreased in comparison with SBA-15, it could be established that calcination temperature of the Pd precursor influences the surface area: for 300°C there was a decrease on the surface area because of pore blocking and decrease of the crystallite size, while for calcination at 200°C, the crystals tend to increase along with porosity increase which is evident from the pore volume changes (0.6 cm^3/g vs 0.9 cm^3/g).

The coverage of HPA on the support can be calculated using the cross-sectional area of the heteropolyacid. For both cases (HPA/SBA-15 and Pd/HPA-300/SBA-15) the coverage is similar with some differences associated mainly with changes in the surface area. Although in these catalytic systems, the same amount of HPA was incorporated on the supports, it has been reported that when HPA coverage increases linearly with HPA loading, a better dispersion of HPA is favored [7]. In addition, the amount of Pd in all the catalysts was estimated using emission spectrocopy, obtaining values close to the amounts used for the synthesis.

3.1.2. XPS

To further investigate the nature of Pd and W species (as well as O and C), XPS spectra were taken and analyzed as shown in Fig. 3. High resolution Pd spectrum for Pd/SBA-15, displayed typical Pd $3d_{5/2}$ and Pd $3d_{3/2}$ signals at 335.6 eV and 340.9 eV, respectively. Difference between both peaks corresponds to 5.38 eV which is close to the reported value for PdO (5.26 eV) [27] and agrees with the methodology used for the catalyst preparation. Interestingly, when heteropolyacid is incorporated, both Pd $3d_{5/2}$ and Pd $3d_{3/2}$ signals were shifted to a slightly larger value. For example, for Pd $3d_{5/2}$ the signal is located at 335.9 eV while for Pd $3d_{3/2}$ it was 341.1 eV. In this case, the difference between both was 5.24 eV being almost the same value as for PdO. Evidently, incorporation of heteropolyacid promotes a slight improvement in the synthesis of PdO particles which agrees with the SEM images (next section). The metallic Pd^0 signal has been reported previously to appear at 335 eV [28], however because of the synthesis procedure not involving any catalyst reduction, this material is composed mainly of PdO rather than metallic Pd. On the other hand, it was observed that for Pd/SBA-15 the signals are slightly less intense compared to Pd/HPA/SBA-15. This fact is indicative of possible amounts of PdO incorporated over Pd/HPA/SBA-15 catalyst.

In the same way, Fig. S6 illustrates the Pd 3d region of Pd/HPA/SBA-15 catalyst evidencing a high signal-to-noise ratio with a hint on the typical bands of Pd (II). Subsequently, presence of PdO on the surface of this catalyst is not apparent.

The W 4d high resolution survey (Fig. S2 in Supplementary Information) shows the typical signals at around 255 and 243 eV which is a strong evidence for the presence of i) heteropolyacid-like structure and ii) W with the 4+ oxidation state.

3.1.3. SEM and TEM

Fig. 4 presents some selected images (SEM) for Pd-based catalysts. As can be seen, in the case of Pd/HPA/SBA-15 material (Fig. 4a), some small particles are observed with a non-homogeneous distribution. Across the surface some non-regular particles are seen between the zones divided for spaces typical for SBA-15. Upon decreasing the metal loading in Pd/HPA/SBA-15 (i.e. 0.5 wt% of Pd) agglomerates of particles together with regular and uniform shapes are observed (Fig. 4b). Regarding this result and considering the scale of the micrograph it appears that Pd deposition procedure can directly affect the shape and dispersion of the particles, making them more uniform and better shaped when the amount of palladium is low (0.5 wt%). Similarly, Pd/SBA-15 (Fig. 4f) exhibits different shapes of particles in granules with a slight decrease of their size in different directions. It appears that all of them are agglomerated without forming clusters of big sizes. Subsequently, presence of HPA helps to better distribute palladium as seen in Fig. 4a.

When the support was changed to amorphous SiO_2 (Pd/HPA/SiO_2, Fig. 4 c and d), spherical particles are observed typical for silica due to the preparation methodology. A minor coverage in Fig. 4d can be attributed to both HPA and Pd which are impregnated during the catalyst synthesis. This observation illustrates a non-uniform covering of the support. In comparison with the previous catalysts, Pd/HPA-300/SBA-15 (Fig. 4 f and g), for which the heteropolyacid was calcined at 300°C, some rugosity in a random order and growth in different directions could be observed. In some cases, aggregates appear to be in contact forming transversal axis within the framework of the image. In the other case, the apparently canes-like-particles (in white color) are similar to those reported for SBA-15 materials [29].

Evidently, a change in the calcination temperature results in different morphology. Incorporation of both Pd and HPA on silica could affect typical morphology of SBA-15 lowing or elevating the local curvature having an impact on deviations from the spherical shape [30]. In our case (except for Pd/HPA/SiO_2) incorporation of Pd and HPA on

Table 2
Brønsted-to-Lewis ratio for all heterogeneous catalysts.

Catalyst	*Acidity (Brønsted-to-Lewis ratio)*		
	Weak	***Medium***	***Strong***
Pd/SBA-15	0.17	0.12	0.29
HPA/SBA-15	-	0.38	4.12
Pd/HPA/SBA-15	1.03	0.70	1.29
Pd/HPA-300/SBA-15	1.43	-	-
Pd/HPA/SiO_2	0.48	-	-

Table 3
Catalytic activity of the multifunctional catalysts in the allylic oxidation of β-pinene.

Catalyst	*X (%)*	S_{Pcvol}	S_{Pcam}	S_{Mol}	S_{other}	*TOF* (h^{-1})***
HPA/SBA-15	12	10	9	-	81*	6.4
Pd/SBA-15	0	0	0	0	0	0
Pd/HPA	96	20	5	12	63*	18.2
Pd/HPA/SBA-15	78	66	8	17	9	9.9
Pd/HPA-300/SBA-15	99**	63	12	16	9	18.1
Pd(0.5)/HPA/SBA-15	90**	67	13	15	5	33.8
Pd/HPA/SiO_2	17	53	17	18	12	3.2

Reaction conditions: 20 mg of catalyst with d_p<45 μm, 1 mmol of β-pinene, 6.8 mmol of H_2O_2, acetone as solvent (1 mL), 50°C, 18 h, toluene as internal standard. Uncertainty ~2%.

* Mainly isomers of β-pinene.

** 15 mg of catalyst.

***TOF= mmol of β-pinene converted per mmol of active sites (mmol of HPA plus mmol of Pd) over time.

SBA-15 increases the local curvature energy resulting in particles with a cane-like-shape rather than typical spherical particles. The EDX spectra of these materials (Figs. S8 and S9, Supporting Information) demonstrated that loading of Pd species (in both atomic and weight percentage) is slightly higher than W in the case of the material calcined at 200°C compared to 300°C, suggesting that calcination temperature affect the deposition of both W and Pd. In general, after calcination of a heteropolyacid at 200°C it can be more easily embedded into SBA-15 forming non-spherical particles and increasing the curvature energy.

The metal dispersion was measured for one of the most representative catalysts by using TEM. The TEM image in Fig. 5 highlights Pd nanoparticles present in Pd/HPA/SBA-15. As can be seen, the typical channels together with the pores are visible in the images along with the well dispersed Pd particles which showed a size of 7.1 ± 2.1 nm.

3.1.4. Acidity by FTIR using pyridine as a probe molecule

Catalyst acidity and the acid strength distribution are important markers for different reactions, including allylic oxidation of terpenes. In this research, acidity was measured by using pyridine as a probe molecule for Brønsted and Lewis acid sites. The band at ca. 1455 cm^{-1} is associated with the Lewis acid sites while the band at 1545 cm^{-1} is mainly related to Brønsted sites [8]. In this case, Lewis acid sites correspond to Pd and W metal centers while Brønsted sites results from interaction of pyridine within the typical protons coming from hydroxyl (typical in metal oxides). Table 2 contains the Brønsted to Lewis ratio for some selected samples investigated during this research. Pd/SBA-15 displayed acid sites of various strength. Low presence of Brønsted sites in Pd/SBA-15 with a weak strength could be related to surface hydroxyl groups typical for SBA-15 exhibiting weak acidity [31]. In general, in silica based materials, the Brønsted behavior originates from pseudo-bridging silanols which are formed from Si-OH environment [32].

Interestingly, acidity in Pd/HPA/SBA-15 looks slightly different in comparison with HPA/SBA-15 or Pd/SBA-15. It seems that similar amounts of weak and strong Lewis and Brønsted sites can be explained by compensation of the loss of bridging Si-O-Si (Si-OH) bonds with the heteropolyacid (HPA). A different behavior is clearly observed for medium acid sites. Particularly, a major content of Lewis sites is observed indicating that incorporation of HPA directly affected such acid sites contrary to weak and strong acid sites. On the other hand, for Pd/HPA/SiO_2, acidity appears to be only of weak strength with a high content of Lewis type. A switch from SBA-15 to SiO_2, dramatically changes the acidity behavior, which could be attributed to the surface area decrease and different distribution of Pd and HPA across different supports.

3.2. Catalytic activity

3.2.1. Screening of multifunctional catalysts

Catalytic activity of the multifunctional catalysts used in the allylic oxidation of β-pinene is illustrated in Table 3.

Blank experiments without a catalyst and with the supports only (i.e. SBA-15 and SiO_2) did not result in either significant conversion or high selectivity to one of the desired targets (<3%).

Experiments with HPA/SBA-15 an Pd/SBA-15 gave 12% conversion with a poor selectivity to *trans*-pinocarveol and pinocamphone and mainly formation of β-pinene isomers. On the other hand, Pd/SBA-15 did not display any catalytic activity. It is well known that although HPA is a strong Brønsted acid itself when deposited on SBA-15, acidity decreased giving values of acidity up to 187 μmol/g_{cat}, which is sufficient to isomerize β-pinene [33]. An experiment with HPA/SBA-15 for pinene transformations without addition of an oxidizing agent gave only isomerization products (conversion >99%). Upon addition of an oxidizing agent conversion decreased while selectivity to pinene isomers remained the same. Absence of catalytic activity in the case of Pd/SBA-15 could be attributed to its low Brønsted acidity with low strength. Although acidity is not the main criterion for this reaction, activation of hydrogen peroxide (oxidizing agent) and its adsorption on the metal modified support have been invoked to explain both the decomposition of hydrogen peroxide and formation of the oxidation products [34]. In the same way, hydrogen peroxide may form relatively strong hydrogen bonds preventing efficient interactions with β-pinene and thus low activity of Pd/SBA-15, HPA/SBA-15 and even Pd/HPA/SiO_2.

When Pd was supported on HPA exhibiting a low surface area of 3 m^2/g, a high conversion (up to 96%) was achieved at the same time with poor selectivity to *trans*-pinocarveol. High activity could be attributed to a high acid density while poor selectivity to the oxidation products is related to the low surface area, poor hydrogen peroxide activation and possibly presence of strong acid sites. It can be concluded that strong Brønsted acid sites increase formation of isomers rather than the oxidized products.

In general, combination of Pd together with SBA-15 did not afford reasonable activity while Pd/HPA and HPA/SBA-15 were active but not selective to the desired products. Subsequently a combination of both Pd, HPA and SBA-15 appears to be promising to achieve high yields of the desired compounds. Pd catalysts supported on HPA, and SBA-15 have been therefore prepared and evaluated in the catalytic oxidation of β-pinene. As expected, these catalysts synthesized by varying the calcination temperature or the amount of palladium exhibited rather high yields of *trans*-pinocarveol. Changes in the calcination temperature or even the amount of palladium (up to 1 wt%) did not have a significant impact on the performance.

Because of the nature of each catalyst, the values of TOF were calculated considering the amounts of palladium and HPA as active catalytic species. In comparison with all catalysts, the values of TOF were higher in the case of the multifunctional materials comprising HPA and Pd supported on SBA-15, while HPA/SBA-15, Pd/HPA/SiO_2 and Pd/SBA-15 did not display high values of TOF. Note that Pd/HPA exhibited one of the highest TOF values, however, with poor selectivity to the oxidation products.

A decreasing of the catalytic activity was observed at higher calcination temperatures and with lower amounts of Pd. The maximum value

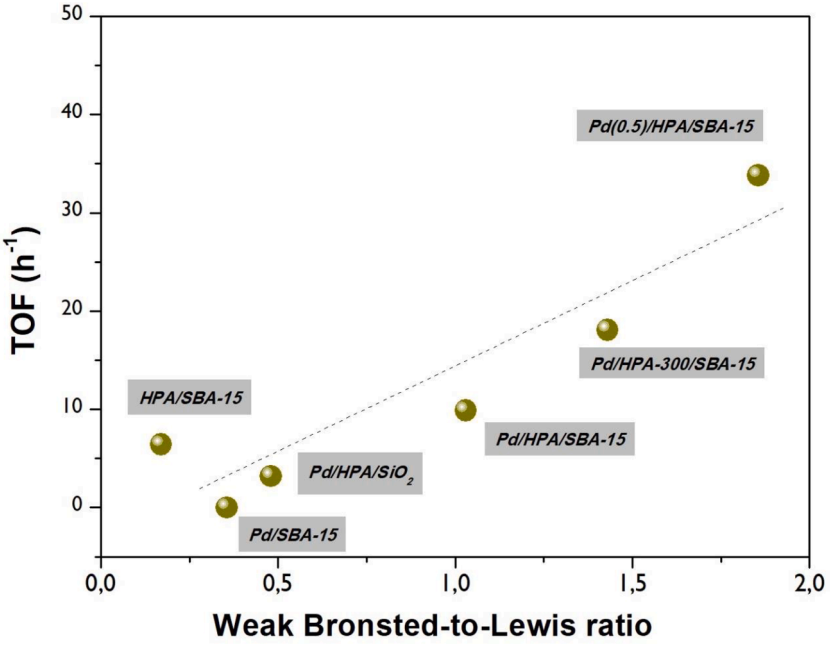

Fig. 6. TOF as a function of the ratio of weak Brønsted-to-Lewis ratio acid sites for different catalysts.

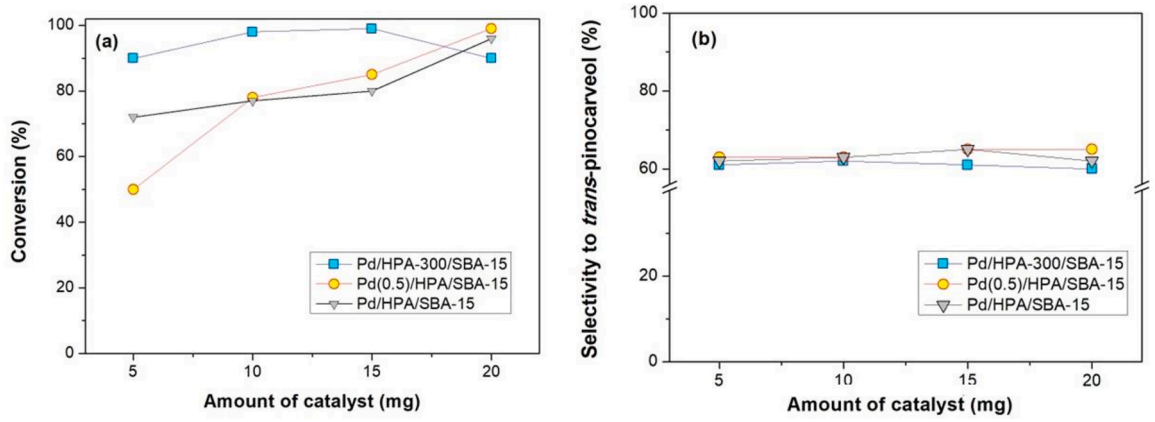

Fig. 7. Effect of the catalyst mass on (a) conversion and (b) selectivity to *trans*-pinocarveol. Reaction conditions: 1 mmol of β-pinene, 6.8 mmol of H_2O_2, acetone as a solvent (1 mL), 50°C, 18 h, toluene as an internal standard.

of TOF (33.8 h^{-1}) was achieved for Pd(0.5)/HPA/SBA-15 whereas a value of 18.1 h^{-1} was achieved for Pd/HPA-300/SBA-15 catalyst. To further compare both Pd catalysts, the initial reaction rates were calculated indicating that lower Pd amounts and calcination temperature were beneficial (0.32 mmol/g min vs 0.24 mmol/g min for Pd(0.5)/HPA/SBA-15 and Pd (1.0)/HPA-300/SBA-15 respectively). Interestingly, both catalysts presented similar surface coverage (0.1350 vs 0.1160 for Pd(0.5)/HPA/SBA-15 and Pd (1.0)/HPA-300/SBA-15 respectively) which affects slightly the initial reaction rate.

With the aim to unravel the properties that affect catalytic oxidation of β-pinene, the TOF was plotted vs different catalytic descriptors. In particular TOF as a function of the ratio of Brønsted-to-Lewis acid sites (Fig. 6) displayed a clear correlation giving a linear increase of TOF with the largest value for Pd(0.5)/HPA/SBA-15. As expected, the minimum values of TOF were achieved for HPA/SBA-15, Pd/SBA-15 and Pd/HPA/SiO_2 catalysts.

It can be speculated that on weak sites adsorption of the oxidizing agent hydrogen peroxide is not strong allowing it to be co-adsorbed with β-pinene. The latter is essential in generation of the carbocations crucial for allylic oxidation to *trans*-pinocarveol.

In general, it appears that not only the weak Brønsted-to-Lewis ratio but also morphology are crucial for achieving selective *trans*-pinocarveol formation. On the other hand, high Brønsted acidity leads to skeletal rearrangement giving isomers as reported previously [35]. More detailed studies on the effect of reaction conditions were carried out for the catalysts which showed the best catalytic performance for synthesis of *trans*-pinocarveol.

3.2.2. *The effect of the reaction parameters*

Catalyst mass. Results on the oxidation of β-pinene are shown in Fig. 7.

In the case of Pd/HPA-300/SBA-15, an increase of the catalyst mass (up to 15 mg) showed a slight increase of the conversion, which was in fact rather high being thus almost independent on the catalyst mass. Selectivity to all products remains unaffected giving *trans*-pinocarveol as the main product. For Pd(0.5)/HPA/SBA-15 with lower Pd content and the calcination temperature a more pronounced effect was observed giving an almost linear behavior.

With these results is also evident that selectivity to *trans*-pinocarveol is almost the same regardless of the temperature calcination and the

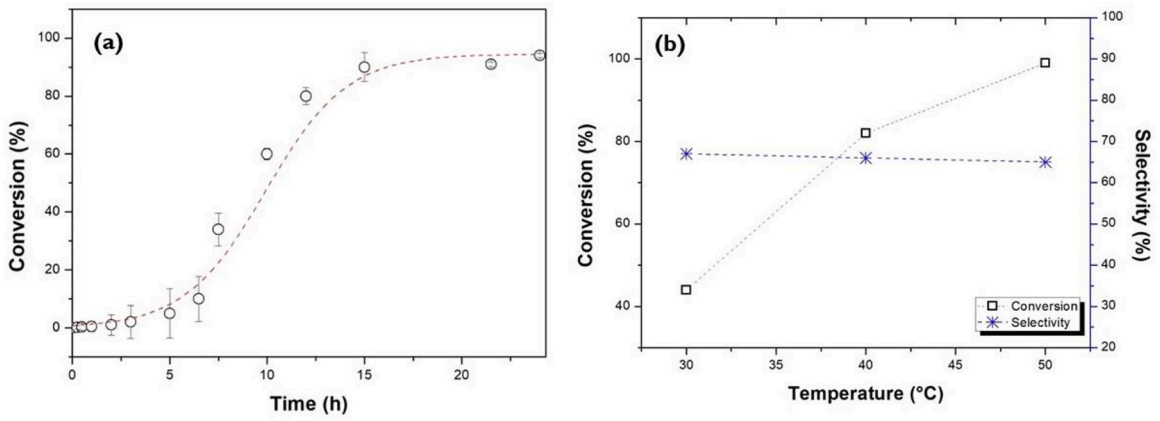

Fig. 8. Dependence of β -pinene conversion over Pd/HPA-300/SBA-15 with (a) time at *50°C* and (b) temperature after 18 h. *Reaction conditions: 20 mg of catalyst, acetone as a solvent, toluene as an internal standard, $d_p < 45$ μm. Measurements were performed as duplicates.*

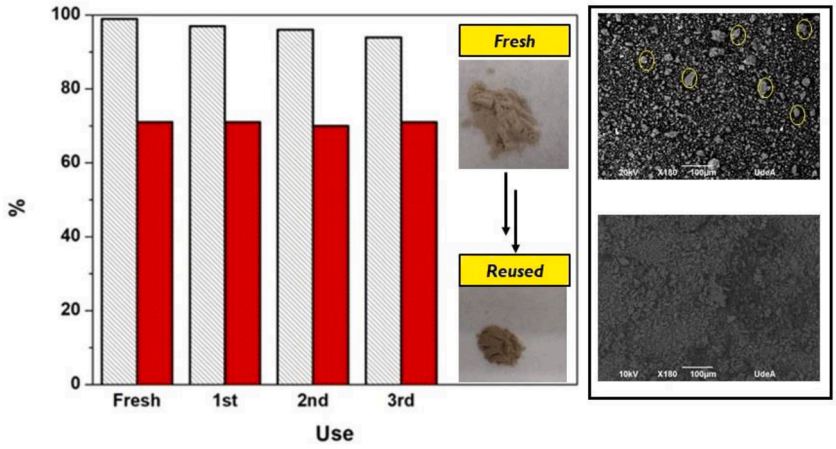

Fig. 9. Reuse of the catalyst Pd/HPA-300/SBA-15. Gray color indicate conversion while red is the selectivity to *trans*-pinocarveol. In the right it is showed the color of the catalyst fresh and reused and SEM images before and after the reaction. ***Reaction conditions:*** *20 mg of catalyst, 0.05 mmol of β-pinene, acetone as a solvent, 50°C, 18 h, toluene as an internal standard, $d_p < 45$ μm.*

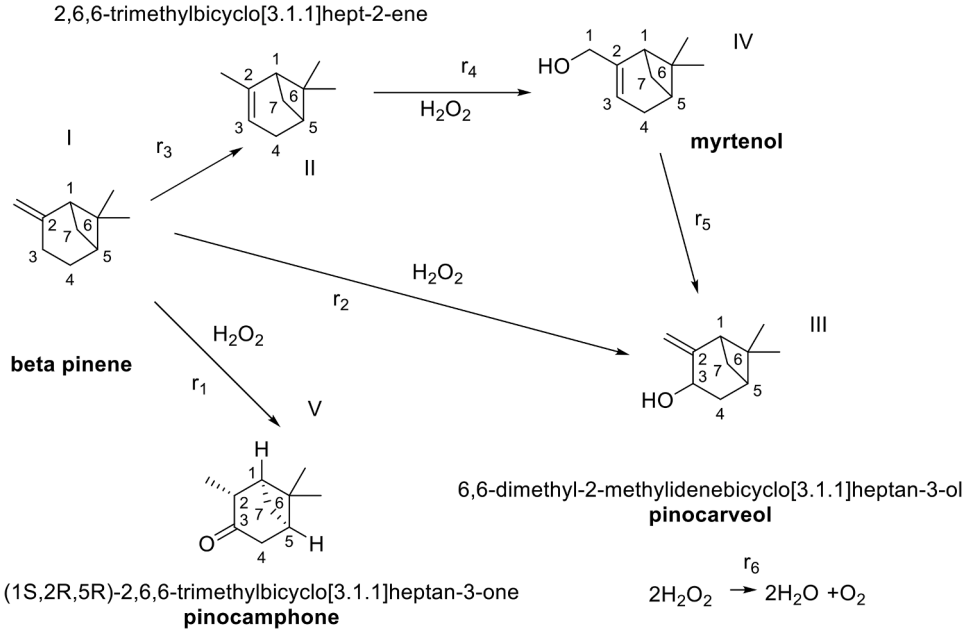

Fig. 10. Reaction network in oxidation of β-pinene.

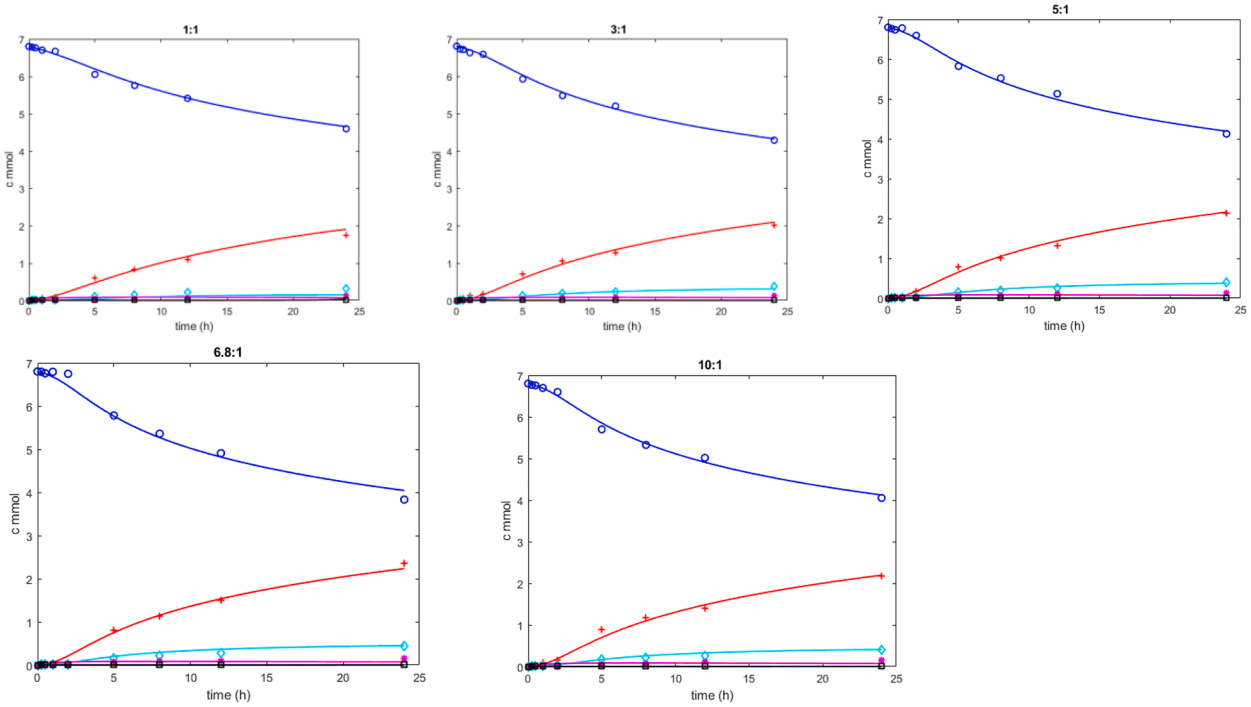

Fig. 11. Comparison between experimental and calculated values.

Table 4
Values for kinetic parameters and statistical analysis.

Parameter	*Value*	*Units*	*Standard error (%)*
$k_1\rho_b$	0.024	h^{-1}	>100
$k_2\rho_b$	0.045	h^{-1}	>100
$k_3\rho_b$	684	mol/L/h	>100
$k_4\rho_b$	7.1	h^{-1}	>100
$k_5\rho_b$	1.35	mol/L/h	15
$k_6\rho_b$	$8\ x10^{-3}$	h^{-1}	27
K_I	$1.9x10^{-4}$	L/mol	>100
K_{II}	0.95	L/mol	14
k'_1	$2.3x10^{3}$	h^{-1}	>100
n	1		

ρ_b is the catalyst bulk density, equal to 15 mg.mL^{-1}.

amount of Pd. Subsequently a multifunctional catalyst based on heteropolyacid and palladium and dispersed on a structured silica is efficient in achieving high yields of *trans*-pinocarveol. The observation of product distribution almost independence on conversion will be used below in kinetic modelling.

Effect of the hydrogen peroxide to β-pinene ratio on the catalytic performance. Hydrogen peroxide amount is crucial for the oxidation of alkenes influencing activity and selectivity. Different ratios of hydrogen peroxide to monoterpene were investigated (1:1, 3:1 and 6.8:1) and the results did not show major differences in the conversion of β-pinene and selectivity to *trans*-pinocarveol using the selected heterogeneous catalysts. Under H_2O_2 lean conditions (H_2O_2: β-pinene=1:1) selectivity to *trans*-pinocarveol was up to 70% at total conversion after 17 h of the reaction. A similar behavior was observed when the ratio was increased up to 6.8:1 over all catalysts without an apparent increase of the byproducts in line with the data on oxidation of cyclohexene over acidic V_2O_5/MoO_3 catalyst [36]. It appears that over tested catalysts, degradation of hydrogen peroxide at ambient temperatures was minimal not influencing conversion and selectivity.

Effect of the time and temperature. A separate experiment was performed to investigate the time dependence of concentration using Pd/HPA-300/SBA-15 catalyst and increasing the amount of all reactants and the solvent fivefold to ensure sufficient quantity of the reaction mixture for sampling. The data are presented in Fig. 8 for β-pinene conversion vs time.

As can be expected, conversion of the monoterpene increases with time until almost completion (99%). A typical S shape in the plot can be observed in Fig. 8 pointing out on some sort of autocatalysis. The effect of temperature was also explored using the most promising catalytic system. For this purpose and considering the boiling point of the solvent (acetone, 56°C) three different temperatures were evaluated. As can be seen from Fig. 8b, conversion increased from 42% at 30°C to 98% at 50°C. Selectivity to *trans*-pinocarveol was almost constant with a slight decrease from 68% to 65% upon temperature increase, which implies that activation energy in parallel pathways is close to each other.

3.2.3. Reuse of the catalyst

Considering the importance of the robustness of a heterogeneous material, the catalyst Pd/HPA-300/SBA-15 was separated from the reaction medium and then reused for several catalytic runs. For this, the catalyst was washed with a mixture of acetone/ethyl acetate and dried at 100°C overnight and reused. Drying was preferred over calcination because HPA at high temperatures tends to decompose into WO_X and PO_x oxides not active in the reaction. Fig. 9 illustrates that the catalyst can be reused for several times with a slight decrease of the conversion keeping, however, the same selectivity to *trans*-pinocarveol.

Based on these results, it is possible to conclude that the material is reasonably robust and reusable without substantial changes in catalytic activity. According to SEM images some agglomerates of the particles in the fresh sample disappear after the catalytic runs, moreover the color of the solid change slightly. The latter can be attributed to deposition of organic compounds which are not totally removed after washing and drying.

Leaching test was performed to identify the possible loss of heteropolyacid or Pd from the catalyst. The reaction was performed at similar reaction conditions (15 mg of catalyst, 0.05 mmol of β-pinene, acetone

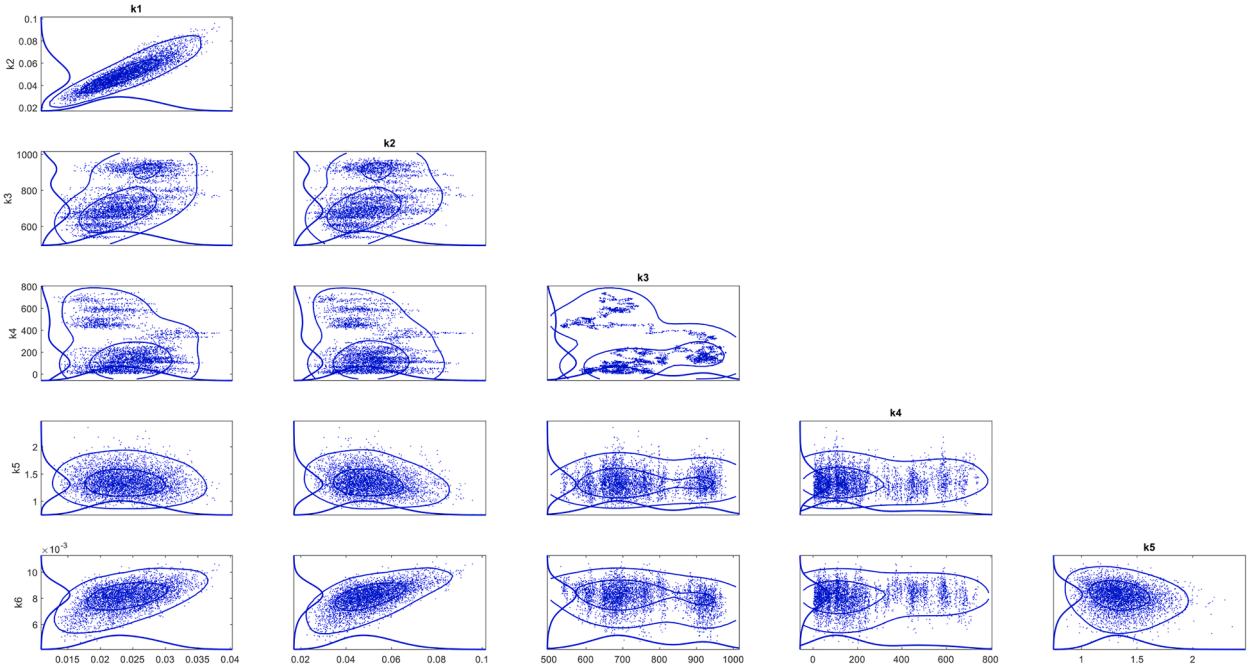

Fig. 12. Contour plots for all parameter combinations.

as a solvent, 50°C, toluene as an internal standard, d_p<45 μm) for 3 h and then the catalyst was removed by hot filtration while the supernatant was constantly stirred for another 2 h. The results showed the increase in the substrate conversion suggesting a slight leaching of both heteropolyacid and Pd of the material. Conversion at 3 h was 50% while at 5 h (after removal of the catalyst) was 55%. Fluorescence analysis together with emission atomic spectroscopy showed a decreasing of both Pd and W in the reused material. A Pd/W ratio of 0.32 was achieved in the fresh material while 0.52 was obtained after reuses. In addition, in the fresh sample the amount of Pd was 1.8% while in the reused catalyst was 0.85% showing a considerable loss in the Pd amount during all the catalytic cycles.

3.2.4. Kinetic modelling

Kinetic modelling of this reaction was performed with the aim to elucidate the determining steps as well as possible reaction pathways in the allylic oxidation of β-pinene. For this, the reaction network was proposed (Fig. 10).

In Fig. 10 reactions 1, 2 and 4 require presence of hydrogen peroxide as an oxidizing agent, while reactions 3 and 5 are irreversible double bond migration and isomerization reactions. For the sake of simplicity not only the oxidation reactions (1, 2 and 4), but also isomerization reactions were assumed to be irreversible. In addition to reactions involving organic compounds, decomposition of hydrogen peroxide was also considered (reaction 6 in Fig. 10).

Because of the S-shape behavior of the concentration curves, the kinetic model was selected using the cooperative kinetics approach [36], where for the Eley-Rideal type of mechanism for the reaction A+B→C the following rate expression was proposed.

$$r=\frac{\left(k_A K_{0A} C_A+2k_{AA} K_{0A} K_{AA} C_A^2+\left(k_{AC} K_{AC} K_{0A}+k_{CA} K_{CA} K_{0C}\right) C_A C_C\right) C_B}{1+K_{0A} C_A+K_{0A} K_{AA} C_A^2+\left(K_{AC} K_{0A}+K_{CA} K_{0C}\right) C_A C_C+K_{0C} C_C+K_{0C} K_{CC} C_C^2} \quad (1)$$

In Eq. (1) k and K correspond to reaction and adsorption constants, which depend on the spatial arrangement of reacting molecules, namely presence of another reacting molecule or the product on the catalyst surface. In this treatment it was assumed that on a nanocluster of a metal only a limited number of bulky organic molecules can be adsorbed. To simplify kinetic analysis, it can be suggested that molecules with the double bond in the ring, as well as pinocamphone have lower affinity to the catalyst surface compared with β-pinene and pinocarveol. In this case Eq. (1) can be directly used for the first reaction in Fig. 10 taking the form:

$$r_1=\frac{\left(k_{1,I} K_{0I} C_I+2k_{1,I\_I} K_{0I} K_{I\_I} C_I^2+\left(k_{1,I\_III} K_{I\_III} K_{0I}+k_{1,III\_I} K_{III\_I} K_{0III}\right) C_I C_{III}\right) C_{H_2O_2}}{1+K_{0I} C_I+K_{0I} K_{I\_I} C_I^2+\left(K_{I\_III} K_{0I}+K_{III\_I} K_{0III}\right) C_I C_{III}+K_{0III} C_{III}+K_{0III} K_{III\_III} C_{III}^2} \quad (2)$$

Where compounds I and III correspond to β-pinene and pinocarveol respectively. Eq. (2) reflects the case of only two adsorbed species per metal cluster and assumes that the clusters have different reactivity depending on the sequence of adsorption steps, thus recognizing the difference in adsorption constants K_{I_III} and K_{III_I}. In the case of non-distinguishable clusters and if lateral interactions depend only on the presence of a second substrate on a cluster, but not on the nature of this second substrate (meaning that $k'_1 = k_{1,I\_I} = k_{1,I\_III} = k_{1,III\_I}$) Eq. (2) can be simplified to

$$r_1=\frac{k_1 K_I C_I C_{H_2O_2}+k'_1\left(2K_I^2 C_I^2+2K_I K_{III} C_I C_{III}\right) C_{H_2O_2}}{1+K_I C_I+K_I^2 C_I^2+2K_I K_{III} C_I C_{III}+K_{III} C_{III}+K_{III}^2 C_{III}^2} \quad (3)$$

In a similar way the rate expressions for reactions 2 and 3 are

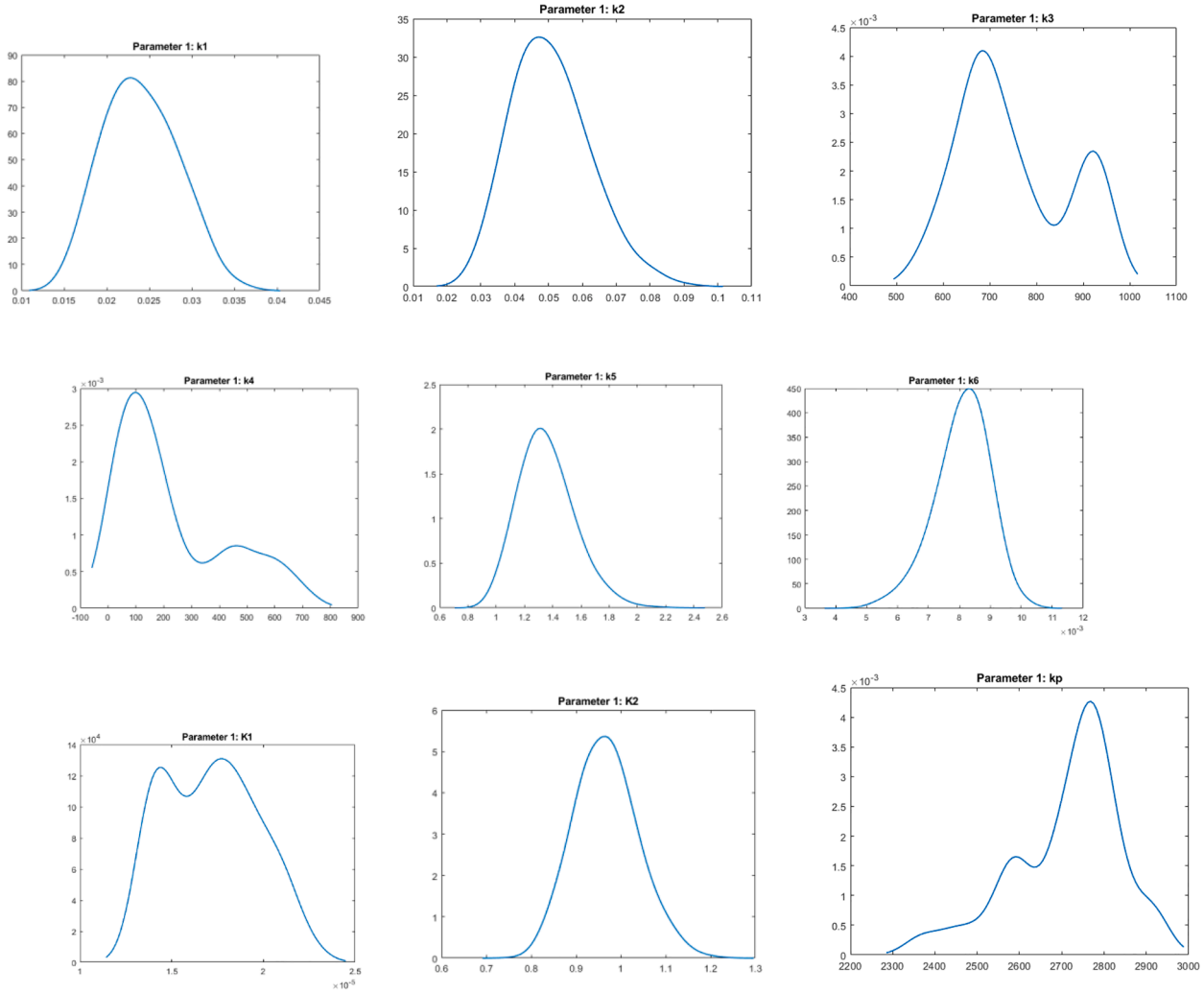

Fig. 13. MCMC analysis of parameters determined by nonlinear regression. The X- axes correspond to values of parameters, while Y-axes reflect the probability of parameters and correspond to their posterior distributions.

$$r_2 = \frac{k_2 K_I C_I C_{H_2O_2} + k_2^{'}\left(2K_I^2 C_I^2 + 2K_I K_{III} C_I C_{III}\right) C_{H_2O_2}}{1 + K_I C_I + K_I^2 C_I^2 + 2K_I K_{III} C_I C_{III} + K_{III} C_{III} + K_{III}^2 C_{III}^2} \tag{4}$$

$$r_3 = \frac{k_3 K_I C_I + k^{'}{}_3\left(2K_I^2 C_I^2 + 2K_I K_{III} C_I C_{III}\right)}{1 + K_I C_I + K_I^2 C_I^2 + 2K_I K_{III} C_I C_{III} + K_{III} C_{III} + K_{III}^2 C_{III}^2} \tag{5}$$

Note absence of hydrogen peroxide concentration in Eq. (5). For the rates of other reactions in the reaction network, namely reactions 4 and 5, due to low affinity of compounds II and IV it can be assumed that their coverage is substantially lower than for adsorbed pinene and pinocarveol. Subsequently adsorbed compound II can react being located on a cluster without a neighboring adsorbed molecule or when either β-pinene or pinocarveol are adsorbed. This leads to the following rate expression of reaction 4.

$$r_4 = \frac{k_4 K_{II} C_{II} C_{H_2O_2} + k_4^{'}(K_I K_{II} C_I C_{II} + K_{II} K_{III} C_{II} C_{III}) C_{H_2O_2}}{1 + K_I C_I + K_I^2 C_I^2 + 2K_I K_{III} C_I C_{III} + K_{III} C_{III} + K_{III}^2 C_{III}^2} \tag{6}$$

And similarly, reaction 5

$$r_5 = \frac{k_5 K_{IV} C_{IV} + k_5^{'}(K_I K_{IV} C_I C_{IV} + K_{III} K_{IV} C_{III} C_{IV})}{1 + K_I C_I + K_I^2 C_I^2 + 2K_I K_{III} C_I C_{III} + K_{III} C_{III} + K_{III}^2 C_{III}^2} \tag{7}$$

For hydrogen peroxide decomposition a semi-empirical power low model was applied, giving eventually the reaction order in hydrogen peroxide equal to unity based on the data fitting.

$$r_6 = k_6 C_{H_2O_2}^n \tag{8}$$

The catalyst bulk density is implicitly incorporated in the rate constants. The generation rates of components of the reaction network can be easily written.

$$-\frac{dC_I}{dt} = r_1 + r_2 + r_3,\ \frac{dC_{II}}{dt} = r_3 - r_4,\ \frac{dC_{III}}{dt} = r_2 + r_5,\ \frac{dC_{IV}}{dt} = r_4 - r_5,\ \frac{dC_V}{dt} = r_1,\ -\frac{dC_{H_2O_2}}{dt} = r_1 + r_2 + r_4 + r_6 \tag{9}$$

The parameter estimation was carried out with a software ModEst [37]. The objective function taken as the squared difference between the experimental and calculated values was minimized by using hybrid simplex and Levenberg-Marquardt algorithms resulting in a very good description of the experimental observations. Preliminary analysis demonstrated that the system is overparametrized and some simplifications can be made, namely that $k_2^{'} = k_2^{'}, k_3^{'} = k_3^{'}; k_4^{'} = k_4^{'}; k_5^{'} = k_5^{'}$, and $K_{II} = K_{III} = K_{IV}$. The coefficient of determination R^2, which compares the model performance with respect to the variance of all experimental points, was 99.94% for this case with mentioned above simplifications. The calculation results demonstrated in Fig. 11 illustrate a good description of the experimental data at different hydrogen peroxide to the substrate ratio.

As can be seen from Fig. 11 the model is capable of capturing the so-called S-shape behavior of the concentration profiles. The values of parameters along with the corresponding errors are shown in Table 4, demonstrating, however, rather large errors for the majority of parameters.

As apparently clear from Table 4 the constants are not statistically reliable, therefore the Markov Chain Monte Carlo analysis [38] has been performed to find the most probable values of parameters. This method, incorporated in the modelling software ModEst, allows an evaluation of the reliability of the model parameters by treating all the uncertainties in the data and in the modelling as statistical distributions. As follows from Fig. 12 displaying contour plots for all parameter combinations, the correlations visible from an elongated shape are apparent for k_1 and k_2.

Despite the large estimated errors for the rate and adsorption constants (Table 4) the MCMC analysis (Fig. 13) confirms rather well defined maxima for the majority of parameters allowing a possibility of their mechanistic interpretation. In particular a rather low rate constant for hydrogen peroxide decomposition should be noted. Moreover, a large difference in the absolute values between $k_1^{'}$ and k_1 points out on lateral interactions as a reason for the S-shaped behavior of concentration profiles.

4. Conclusions

Selective oxidation of β-pinene for synthesis of *trans*-pinocarveol was carried out successfully using a multifunctional heterogeneous catalyst containing both an acid and metal functions (Pd/HPA/SBA-15). Both Pd and the heteropolyacid played an important role in the reaction avoiding formation of epoxidation or condensation products. It was demonstrated that also the nature of the support (i.e.: SiO_2 vs SBA-15) influenced the yield of *trans*-pinocarveol. Higher acidity favored formation of the isomerization products. Absence of the inorganic support (case of Pd/HPA) resulted in a high conversion but poor selectivity to *trans*-pinocarveol as strong Brønsted acidity led to isomerization at the expense of oxidation products. An increase of the weak Brønsted acid sites together with a typical parallelogram-like particle shape are responsible for formation of the desired product. Selectivity to the desired pinocarveol does not depend strongly on the monoterpene conversion. The concentration dependence on time displayed a typical S-shape behavior which was quantitatively modelled for different ratios of pinene and hydrogen peroxide displaying a very good correspondence between the experimental and calculated data.

Overall, the multifunctional catalyst Pd/HPA/SBA-15 developed in the current work was efficient to achieve high yields of *trans*-pinocarveol.

CRediT authorship contribution statement

Julián E. Sánchez-Velandia: Conceptualization, Methodology, Formal analysis, Investigation, Writing – original draft, Project administration. **Laura M. Valdivieso:** Validation, Formal analysis, Investigation. **Fernando Martínez O:** Formal analysis, Resources, Writing – review & editing, Supervision, Funding acquisition. **Sol M. Mejía:** Formal analysis, Resources, Writing – review & editing, Supervision, Funding acquisition. **Aída L. Villa:** Formal analysis, Investigation, Formal analysis, Resources, Writing – review & editing, Supervision. **Johan Wärnå:** Conceptualization, Methodology, Software, Investigation. **Dmitry Yu. Murzin:** Conceptualization, Methodology, Software, Investigation, Writing – review & editing.

Declaration of Competing Interest

The authors declare that they have no known competing financial interests or personal relationships that could have appeared to influence the work reported in this paper.

Data availability

Data will be made available on request.

Acknowledgements

This research was partially supported by Ministerio de Ciencia, Tecnología e Innovación, Ministerio de Educación Nacional, Colombia; Ministerio de Industria, Comercio y Turismo, Colombia, and ICETEX, Colombia, Programme Ecosistema Científico-Colombia Científica from Fondo Francisco José de Caldas, Colombia; Grant RC-FP44842-212-2018. J.E-S. V is grateful to Dr. Esteban Urrego for his help during analysis of XPS. J.E-S.V and S.M.M. thank Pontificia Unversidad Javeriana towards project ID 20385 for the financial support to "Apoyo a Estancias postdoctorales en la Pontificia Universidad Javeriana". J.E-S.V is also grateful to Universidad Jaume I and Dr. Atte Aho (Abo Akademi University) for providing equipment and performing TEM analysis, respectively. A.L.V acknowledges funding from Universidad de Antioquia.

Supplementary materials

Supplementary material associated with this article can be found, in the online version, at doi:10.1016/j.mcat.2023.113104.

References

[1] A. Malmgren, G. Riley, Biomass Power Generation, Elsevier Ltd., 2012, https://doi.org/10.1016/B978-0-08-087872-0.00505-9.
[2] A. Corma, S. Iborra, A. Velty, Chemical routes for the transformation of biomass into chemicals, Chem. Rev. 107 (2007) 2411–2502, https://doi.org/10.1021/cr050989d.
[3] J. Park, J. Meng, K.H. Lim, O.J. Rojas, S. Park, Transformation of lignocellulosic biomass during torrefaction, J. Anal. Appl. Pyrolysis 100 (2013) 199–206, https://doi.org/10.1016/j.jaap.2012.12.024.
[4] N.F. Salakhutdinov, K.P. Volcho, O.I. Yarovaya, Monoterpenes as a renewable source of biologically active compounds, Pure Appl. Chem. 89 (2017) 1105–1117, https://doi.org/10.1515/pac-2017-0109.
[5] K.A.D. Swift, Catalytic transformations of the major terpene feedstocks, Top. Catal. 27 (2004) 143–155, https://doi.org/10.1023/B:TOCA.0000013549.60930.da.
[6] M. Golets, S. Ajaikumar, J.P. Mikkola, Catalytic upgrading of extractives to chemicals: monoterpenes to "eXICALS, Chem. Rev. 115 (2015) 3141–3169, https://doi.org/10.1021/cr500407m.
[7] L. Frattini, M.A. Isaacs, C.M.A. Parlett, K. Wilson, G. Kyriakou, A.F. Lee, Support enhanced α-pinene isomerization over HPW/SBA-15, Appl. Catal. B Environ. 200 (2017) 10–18, https://doi.org/10.1016/j.apcatb.2016.06.064.
[8] J.E. Sánchez-Velandia, E. Pájaro, A.L. Villa, F. Martínez-O, Selective synthesis of camphene from isomerization of α- and β-pinene over heterogeneous catalysts, Microporous Mesoporous Mater. 324 (2021), https://doi.org/10.1016/j.micromeso.2021.111273.
[9] Y.S. Raupp, C. Yildiz, W. Kleist, M.A.R. Meier, Aerobic oxidation of α-pinene catalyzed by homogeneous and MOF-based Mn catalysts, Appl. Catal. A Gen. 546 (2017) 1–6, https://doi.org/10.1016/j.apcata.2017.07.047.
[10] M.J. Da Silva, L.M.M. Vieira, A.A. Oliveira, M.C. Ribeiro, Novel effect of palladium catalysts on chemoselective oxidation of β-pinene by hydrogen peroxide, Monatshefte Chem. 144 (2013) 321–326, https://doi.org/10.1007/s00706-012-0875-5.
[11] J.V. Coelho, L.C.A. Oliveira, F.C.C. Moura, P.P. De Souza, C.A. Silva, K.B. Batista, M.J. Da Silva, β-pinene oxidation by hydrogen peroxide catalyzed by modified niobium-MCM, Appl. Catal. A Gen 419–420 (2012) 215–220, https://doi.org/10.1016/j.apcata.2012.01.032.
[12] B.S. Gomes, B.P.S. Neto, E.M. Lopes, F.V.M. Cunha, A.R. Araújo, C.W.S. Wanderley, D.V.T. Wong, R.C.P.L. Júnior, R.A. Ribeiro, D.P. Sousa, J. Venes R Medeiros, R.C. M. Oliveira, F.A. Oliveira, Anti-inflammatory effect of the monoterpene myrtenol is dependent on the direct modulation of neutrophil migration and oxidative stress, Chem. Biol. Interact. 273 (2017) 73–81, https://doi.org/10.1016/j.cbi.2017.05.019.
[13] M.R.C. Moreira, M.G. da S.S. Salvadori, A.A.C. de Almeida, D.P. de Sousa, J. Jordán, P. Satyal, R.M. de Freitas, R.N. de Almeida, Anxiolytic-like effects and mechanism of (-)-myrtenol: a monoterpene alcohol, Neurosci. Lett. 579 (2014) 119–124, https://doi.org/10.1016/j.neulet.2014.07.007.
[14] S. Dragomanova, L. Tancheva, M. Georgieva, R. Klisurov, Analgesic and anti-inflammatory activity of monoterpenoid myrtenal in rodents, J. IMAB Annu. Proc.

25 (2019) 2406–2413, https://doi.org/10.5272/jimab.2019251.2406 (Scientific Pap.
[15] M. Lindmark-Henriksson, D. Isaksson, T. Vaněk, I. Valterová, H.E. Högberg, K. Sjödin, Transformation of terpenes using a Picea abies suspension culture, J. Biotechnol. 107 (2004) 173–184, https://doi.org/10.1016/j.jbiotec.2003.10.009.
[16] A.A. De Oliveira, M.L. Da Silva, M.J. Da Silva, Palladium-catalysed oxidation of bicycle monoterpenes by hydrogen peroxide in acetonitrile solutions: A metal reoxidant-free and environmentally benign oxidative process, Catal. Lett. 130 (2009) 424–431, https://doi.org/10.1007/s10562-009-9970-6.
[17] A.L. García-Cabeza, R. Marín-Barrios, F.J. Moreno-Dorado, M.J. Ortega, G. M. Massanet, F.M. Guerra, Allylic oxidation of alkenes catalyzed by a copper-aluminum mixed oxide, Org. Lett. 16 (2014) 1598–1601, https://doi.org/10.1021/ol500198c.
[18] R.W. Friesen, Science of synthesis (Methods of molecular transformation), 2001.
[19] C.M. Crombie, R.J. Lewis, D. Kovačič, D.J. Morgan, T.J.A. Slater, T.E. Davies, J. K. Edwards, M.S. Skjøth-Rasmussen, G.J. Hutchings, The selective oxidation of cyclohexane via *In-situ* H_2O_2 production over supported Pd-based catalysts, Catal. Lett. 151 (2021) 2762–2774, https://doi.org/10.1007/s10562-020-03511-6.
[20] G.U. Mennenga, A.I. Rudenkov, K.I. Matveev, I.V. Kozhevnikov, Oxidative coupling of alkylbenzenes to diaryls catalyzed by the palladium(II)-heteropolyacid system, React. Kinet. Catal. Lett. 5 (1976) 401–406, https://doi.org/10.1007/BF02060886.
[21] R.F. Cotta, K.A. da Silva Rocha, E.F. Kozhevnikova, I.V. Kozhevnikov, E. V. Gusevskaya, Heteropoly acid catalysts in upgrading of biorenewables: cycloaddition of aldehydes to monoterpenes in green solvents, Appl. Catal. B Environ. 217 (2017) 92–99, https://doi.org/10.1016/j.apcatb.2017.05.055.
[22] H. Ocawa, H. Fujinami, K. Taya, S. Teratani, Palladium(II) sulfate-heteropoly acid-catalyzed oxidation of cycloolefins in liquid phase, Bull. Chem. Soc. Jpn. 57 (1984) 1908–1913, https://doi.org/10.1246/bcsj.57.1908.
[23] J.E. Sánchez-Velandia, A.L. Villa, Isomerization of α- and β- pinene epoxides over Fe or Cu supported MCM-41 and SBA-15 materials, Appl. Catal. A Gen. (2019), https://doi.org/10.1016/j.apcata.2019.04.029.
[24] P.K. Gallagher, M.E. Gross, The thermal decomposition of palladium acetate, J. Therm. Anal. 31 (1986) 1231–1241, https://doi.org/10.1007/BF01914636.
[25] N. Fairley, V. Fernandez, M. Richard-Plouet, C. Guillot-Deudon, J. Walton, E. Smith, D. Flahaut, M. Greiner, M. Biesinger, S. Tougaard, D. Morgan, J. Baltrusaitis, Systematic and collaborative approach to problem solving using X-ray photoelectron spectroscopy, Appl. Surf. Sci. Adv. 5 (2021), 100112, https://doi.org/10.1016/j.apsadv.2021.100112.
[26] M.A. Balderas Altamirano, S. Cordero, R. López-Esparza, E. Pérez, A. Gama Goicochea, Importance of pore length and geometry in the adsorption/desorption process: a molecular simulation study, Mol. Phys. 113 (2015) 3849–3853, https://doi.org/10.1080/00268976.2015.1070927.
[27] D. Briggs, X-ray photoelectron spectroscopy (XPS). Handbook of Adhesion, 2nd ed., 2005, pp. 621–622, https://doi.org/10.1002/0470014229.ch22.
[28] V.K. Patel, S. Sharma, Effect of oxide supports on palladium based catalysts for NO reduction by H_2-SCR, Catal. Today 375 (2021) 591–600, https://doi.org/10.1016/j.cattod.2020.04.006.
[29] D. Gao, A. Duan, X. Zhang, K. Chi, Z. Zhao, J. Li, Y. Qin, X. Wang, C. Xu, Self-assembly of monodispersed hierarchically porous Beta-SBA-15 with different morphologies and its hydro-upgrading performances for FCC gasoline, J. Mater. Chem. A 3 (2015) 16501–16512, https://doi.org/10.1039/c5ta03671b.
[30] D. Wang, Z. Hu, G. Peng, Y. Yin, Surface energy of curved surface based on lennard-jones potential, Nanomaterials 11 (2021) 1–15, https://doi.org/10.3390/nano11030686.
[31] A.T.Y. Wolek, M.A. Ardagh, H.N. Pham, S. Alayoglu, A.K. Datye, J.M. Notestein, Creating Brønsted acidity at the SiO_2-Nb_2O_5 interface, J. Catal. 394 (2021) 387–396, https://doi.org/10.1016/j.jcat.2020.10.027.
[32] C. Chizallet, P. Raybaud, Pseudo-bridging silanols as versatile brønsted acid sites of amorphous aluminosilicate surfaces, Angew. Chem. Int. Ed. 48 (2009) 2891–2893, https://doi.org/10.1002/anie.200804580.
[33] J.E. Sánchez-Velandia, H.G. Baldoví, A.Y. Sidorenko, J.A. Becerra, F. Martínez O, Synthesis of heterocycles compounds from condensation of limonene with aldehydes using heteropolyacids supported on metal oxides, Mol. Catal. 528 (2022), https://doi.org/10.1016/j.mcat.2022.112511.
[34] H.H. Kim, H. Lee, D. Lee, Y.J. Ko, H. Woo, J. Lee, C. Lee, A.L.T. Pham, Activation of hydrogen peroxide by a titanium oxide-supported iron catalyst: evidence for surface Fe(IV) and its selectivity, Environ. Sci. Technol. 54 (2020) 15424–15432, https://doi.org/10.1021/acs.est.0c04262.
[35] J.V Coelho, L.C.A. Oliveira, F.C.C. Moura, P.P. de Souza, C.A. Silva, K.B. Batista, M. J. da Silva, β-pinene oxidation by hydrogen peroxide catalyzed by modified niobium-MCM, Appl. Catal. A Gen. 419–420 (2012) 215–220, https://doi.org/10.1016/j.apcata.2012.01.032.
[36] G. Yang, M.D. Huff, H. Du, Z. Zhang, Y. Lei, Increased selectivity for allylic oxidation of cyclohexene using TiO_2 modified V_2O_5/MoO_3 catalysts, Catal. Commun. 99 (2017) 43–48, https://doi.org/10.1016/j.catcom.2017.05.023.
[37] H. Haario, ModEst, The Optimization Software, Profmath, Helsinki, 2001.
[38] D.Y. Murzin, J. Wärnå, H. Haario, T. Salmi, Parameter estimation in kinetic models of complex heterogeneous catalytic reactions using Bayesian statistics, React. Kinet. Mech. Catal. 133 (2021) 1–15, https://doi.org/10.1007/s11144-021-01974-1.